

# JAAS

Accepted Manuscript



This is an *Accepted Manuscript*, which has been through the Royal Society of Chemistry peer review process and has been accepted for publication.

*Accepted Manuscripts* are published online shortly after acceptance, before technical editing, formatting and proof reading. Using this free service, authors can make their results available to the community, in citable form, before we publish the edited article. We will replace this *Accepted Manuscript* with the edited and formatted *Advance Article* as soon as it is available.

You can find more information about *Accepted Manuscripts* in the [Information for Authors](#).

Please note that technical editing may introduce minor changes to the text and/or graphics, which may alter content. The journal's standard [Terms & Conditions](#) and the [Ethical guidelines](#) still apply. In no event shall the Royal Society of Chemistry be held responsible for any errors or omissions in this *Accepted Manuscript* or any consequences arising from the use of any information it contains.

# Comparison of single- and multivariate calibration for determination of Si, Mn, Cr and Ni in high-alloyed stainless steels by Laser-Induced Breakdown Spectrometry

Cite this: DOI: 10.1039/x0xx00000x

Received 00th January 2012,

Accepted 00th January 2012

DOI: 10.1039/x0xx00000x

www.rsc.org/

Sergey M. Zaytsev, Andrey M. Popov, Evgeny V. Chernykh, Raisa D. Voronina, Nikita B. Zorov and Timur A. Labutin

The quantitative analysis of high-alloyed steels by LIBS is usually complicated by overlap of the analytical lines with iron lines due to the complex structure of the emission spectra of each component. To overcome this problem, we compared the two calibration strategies in the current research work. Univariate regression analysis was used for a number of analytical lines of Si, Mn, Ni, and Cr with and without strong spectral interferences with other lines. Several methods of data pre-processing (for example, by normalization using an internal standard or baseline correction) to compensate for matrix effects or the pulse to pulse deviations of the analytical signal have been compared with the calibration curves constructed with the use of peak intensities. As an alternative to the univariate strategy, multivariate calibration based on principal component regression (PCR) was used in this work. We examined two criteria separately to select the most predictive model. The minimal values of relative Root-Mean-Square Error of Cross-Validation (RMSECV, %) provided the best prediction accuracy while the use of the well-known F-criterion reduced the number of principal components up to 4 or 5 for each analyte without significant worsening of prediction capability. The measurements within four spectral windows (210-230 nm, 280-300 nm, 345-365 nm and 400-420 nm) were carried out on a set of 10 standard samples. Univariate calibration for Cr, Ni and Mn provided the best prediction ( $R^2=0.996$ ) if the appropriate reference line could be found and analytical lines were not overlapped with others. The best prediction for Si ( $R^2=0.94$ ) were obtained with the using of peak signal of Si 212.41 nm line without normalization. Otherwise, PCR provided good predictive capability (RMSECV, %=3, 4, 5 and 9 of quantification of Mn, Cr, Ni and Si respectively) in the spectral ranges where numerous matrix lines strongly interfered with analytical lines.

## Introduction

Laser-induced breakdown spectroscopy (LIBS) is an emerging technique for material analysis that is also advancing as a technology as new commercial instruments are becoming available.<sup>1</sup> LIBS provides a non-contact sampling by focused laser radiation with simultaneous detection of radiation of laser-induced plasma. This makes possible a real-time analysis of samples of different origin (aerosols, environmental samples, objects of cultural heritage, coating layers, composite materials, alloys etc) by a field-portable sensor,<sup>2</sup> the elimination or only minimal sample preparation and extremely short analysis time. These advantages of LIBS give an opportunity for rapid direct analysis of materials during operation process, for example, inline LIBS control system of the steel fittings provides 4

measurements per second.<sup>3</sup> Chemical analysis of steels is focused on both impurities and doping components determination. However, numerous interferences typical for high alloyed stainless steel due to extremely complex spectra of main components (Fe, Cr, Ni) complicate analysis. In the field of control of metallurgy process, it is important to solve this problem for reliable and accurate analysis result.<sup>4</sup> Here, we focused on searching the experimental conditions and the appropriate calibration strategy for LIBS determination either metal or non-metal components of high-alloyed steels.

Since the content of components of interest in high-alloy steels is relatively high, the main focus is on the search conditions when one can detect individual emission lines or apply algorithms for their separation. To improve the accuracy of a conventional calibration in spectrochemical analysis, various

methods of spectral data preprocessing are usually employed such as a noise removal,<sup>5</sup> the deconvolution of poor resolved emission lines on individual ones,<sup>6</sup> and different normalization techniques with the use of background signal level, the overall intensity of spectra or the internal standard.<sup>7</sup> It should be borne in mind that the deconvolution of the emission lines considerably complicates data processing, and increases the analysis time, in spite of special automatic deconvolution procedures.<sup>8</sup> Moreover, the accuracy of LIBS determination of silicon in high-alloy steels is still poor without inter-element correction which takes into account the influence of chromium on the intensity of the observed peak.<sup>9</sup>

Multivariate techniques of spectral data analysis applicable to a fast and direct prediction of the sample composition in case of overlapping analytical signals. In most cases, the multivariate data analysis in LIBS was successfully applied for qualitative analysis, e.g. classification of composite samples,<sup>10, 11</sup> explosives<sup>12,13</sup> and organic substances,<sup>14,15</sup> which speciation cannot be done directly by LIBS (polymers, micro-organisms, food, etc.). Spectral data are referred for quantification to as independent data  $X [k,l]$  where  $k$  and  $l$  are the number of samples and variables, respectively, while dependent variables  $Y$  present the elemental concentrations. Training set (a number of samples with known elemental concentrations) is used to create a calibration model relating  $Y$  to  $X$  for prediction of component content in the test set (unknown samples). To separate of data of analytical components and noises two most widespread multivariate algorithms for decomposition of matrix  $X$  are implemented: Principal Component Regression (PCR), and Partial Least Squares regression (PLS-1 or PLS-2). A few of papers describe the use of multivariate calibration for the LIBS analysis of steel, thus Stipe et al<sup>16</sup> limited the quantification to main metallic components only, and in the paper of Sorrentino et al<sup>17</sup> the results of the silicon content prediction showed a sufficient discrepancy with the certified values. In both cases, the multivariate calibration model was built with the use of PLS. At the same time, Thomas and Haaland<sup>18</sup> demonstrated that the best results for content prediction with multivariate calibration model can be obtained for either PLS or PCR for different synthetic data sets. Moreover, Yaroshchuk et al<sup>19</sup> reported that standard PLS and PCR models provided similar prediction accuracy, although there were notably less latent variables in the case of PLS.

What method (multivariate or univariate) can be adjusted to obtain a better prediction? Usual univariate technique includes optimization of temporal conditions to achieve maximal separation from other spectral lines besides maximal signal-to-noise ratio (SNR), while PCR may provide the same accuracy without clear distinguishing of individual signals. In this study we therefore focused on a comparison between several calibration approaches for precise determination of Si, Mn, Cr and Ni in high-alloyed stainless steel by means of LIBS. To allow for this, we estimated a prediction capability of PCR models with the use of different spectral regions containing analytical lines of interest as input data and various number of PC's. It seems to be reasonable to use of PCR for development

of a multivariate calibration model in order to eliminate spectral interferences. Several analytical lines for each element as well as the signals normalized by background, internal standard etc. are checked for univariate calibration strategies.

## Experimental

For analytical measurements we used a typical LIBS setup. Radiation from Q-switched Nd:YAG ( $\lambda = 532$  nm, 8 ns, 60 mJ per pulse) laser was directed by a group of right-angle prisms to an achromatic lens (air-spaced doublet, Thorlabs, USA) with  $F = 150$  mm. A laser beam ( $d=6$  mm) was focused perpendicularly onto the sample surface to be ablated in order to form laser plasma. The emission from the central part of laser-induced plasma was projected by two-lens condenser with the decrease of an image 2:1 onto the slit ( $25 \mu$ ) of the Czerny-Turner spectrometer "HR 320" (ISA Instruments, USA). The center of the plasma plume, lenses, and slit were aligned coaxially. Spectrometer, equipped with ICCD camera "Nanogate-2V" (Nanoscan, Russia), provided resolving power of  $\sim 8000$  at 400 nm. Synch output of the Q-switch triggered ICCD camera. The home-made software in LabVIEW® environment controlled the main parameters of the camera (delay, gate, gain). Data pre-processing (background removing, wavelength calibration, and correction for the sensitivity of the photocathode) was performed after the measurements. For these purposes, background was taken as the minimal intensity in the spectrum. To avoid any changes within spectral data, we did not perform de-noising of spectra. Nevertheless, usual procedure of spectra accumulation to decrease noises was also applied. Here and after, we will use a term of *cleaned spectrum* to designate the spectrum after the pre-processing instead of *raw spectrum*, obtained after measurements, as recommended by Engel et al.<sup>20</sup>

The composition of the used high alloy stainless steel samples (BAM, Germany) is given in **Table 1**.

Table 1. Composition of high-alloyed stainless steels (BAM, Germany), wt.%.

CRM	No	Ni	Mn	Cr	Si
462	C1	12.550	0.740	12.350	0.460
461-1	C2	6.124	0.686	14.727	0.374
462-1	C3	12.850	0.722	11.888	0.463
463-1	C4	10.200	1.400	18.460	0.270
464-1	C5	20.050	0.791	25.390	0.570
465-1	C6	9.240	1.380	17.310	0.405
466-2	C7	10.200	1.311	17.840	0.480
468-1	C8	8.900	1.700	17.960	1.410
475	C9	5.660	0.890	14.140	0.210
284-2	C10	10.720	1.745	16.811	0.537

We collected 20 spectra of each sample after 5 cleaning shots in one point of the sample. In compliance with the recommendations of Tognoni et al<sup>21</sup> we optimized the main experimental parameters of LIBS measurements: laser fluence on a sample and temporal parameters of emission signal

registration (delay after a laser pulse and gate). We adjusted the gain of ICCD camera to avoid blooming. To choose optimal experimental conditions the measurements were performed for the sample C2. Fluence was changed by moving a focus position below the surface of the sample, ensuring the minimal fluctuation of peak signal of the silicon line Si I 212.41 nm. The best values of RSD (8%) and the signal-to-background ratio were obtained at 6 mm below the surface. Therefore, in further measurements we used this configuration. The diameter of the spot was  $\sim 400 \mu$ , and the fluence was approximately  $5 \text{ GW/cm}^2$ . Optimal temporal parameters of Si I 212.41 nm signal registration, providing high signal-to-background and high SNR, were the delay after a laser pulse of  $3.5 \mu\text{s}$  and the gate of  $1 \mu\text{s}$ . The optimal temporal parameters for registration of Mn I 404.13 nm were delay after a laser pulse of  $5 \mu\text{s}$  and gate of  $5 \mu\text{s}$ . Spectra of the sample C2 in two spectral ranges are presented in **Figures 1-3**.

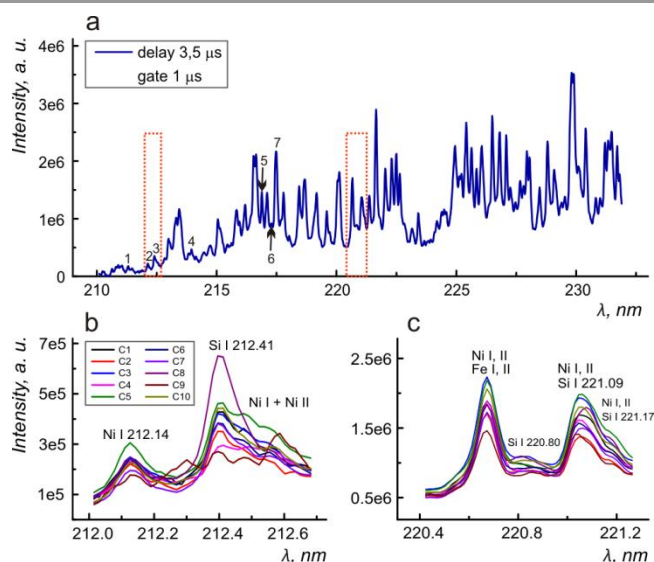


Figure 1. a) Spectrum of the sample C2 in the range 210.1-231.9 nm: Fe I 211.31 nm (1), Ni I 212.14 nm (2), Si I 212.41 nm (3), Fe I 213.97 nm (4), Ni II 216.91 nm (5), Ni II 217.51 nm (6), and Fe I 217.26 nm (7). b-c) The detailed spectra of all studied samples within the ranges marked by red rectangles.

## Results and discussion

### Univariate calibration

Since the number of silicon lines observed in the spectrum of the laser plasma much smaller than the ones of manganese, chromium and nickel, the main efforts were forwarded to analytical signal improvement for silicon determination. Initially, we examined the spectral ranges with often used silicon emission lines Si I 251.61 nm and Si I 288.16 nm. In the first case, the spectral interferences from main components of steels were extremely high, and there was no difference near the expected line of silicon in spectra of samples with the different content of Si. There was strong overlapping with the atomic and ionic lines of chromium in case of Si I line at 288.16 nm. Thus, we accomplished an additional optimization

in this range to obtain the maximal intensity ratio of the Si I 288.16 nm line to sum of Cr II 288.09 and Cr II 288.11 nm lines.

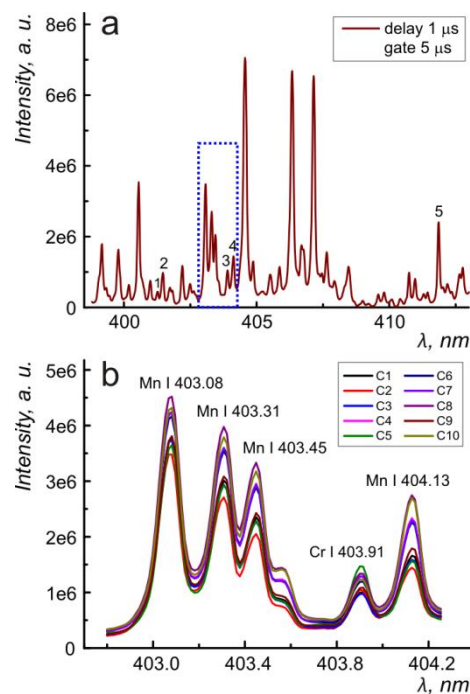


Figure 2. a) Spectrum of the sample C2 in the range 398.8-413.0 nm: Cr I 401.248 nm (1), Fe I 401.453 nm (2), Cr I 403.91 nm (3), and Mn I 404.13 nm (4) and Fe I 411.85 nm (5). b) Spectra of all studied samples in the range marked by blue rectangle.

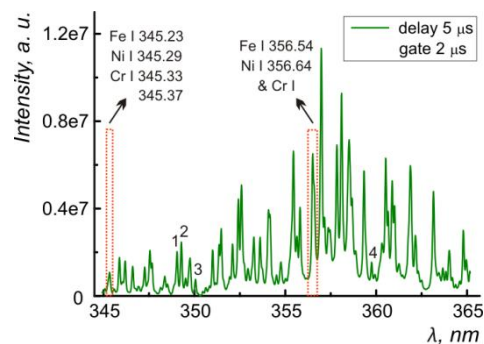


Figure 3. The spectrum of the sample C2 in the range 344.9-365.2 nm: Fe I 349.06 nm (1), Ni I 349.26 nm (2), 350.08 nm (3), 359.77 nm (4). The spectral ranges used for multivariate calibration are marked by red rectangle.

We studied the evolution of silicon and chromium emission lines during an evaporation of a non-alloy steel and high-purity chromium, respectively (gate was fixed to  $2 \mu\text{s}$ , delay was varied from 2 to  $36 \mu\text{s}$  with the step  $2 \mu\text{s}$ ). We found that emissivity of Cr lines decays faster than the ones of Si lines (see **Figure 4,a**). At the same time SNR of Si line was decreased from 16 at  $26 \mu\text{s}$  to 4 at  $36 \mu\text{s}$ . Therefore, the delay time for spectra registration was chosen as late as far the signal of Si line was observed with the high SNR (delay  $26 \mu\text{s}$  and gate  $10 \mu\text{s}$ ). Resulting SNR was equal to 84 for the sample with minimal Si content (C9). Spectra obtained for these temporal parameters in the range 287.5-288.5 nm are presented in **Figure 4,b**. Additional optimization allowed obtaining a linear

calibration, however, the linearity was still insufficient (Table 2) for quantitative determination of silicon. This is due to the influence of Cr lines even after optimization.

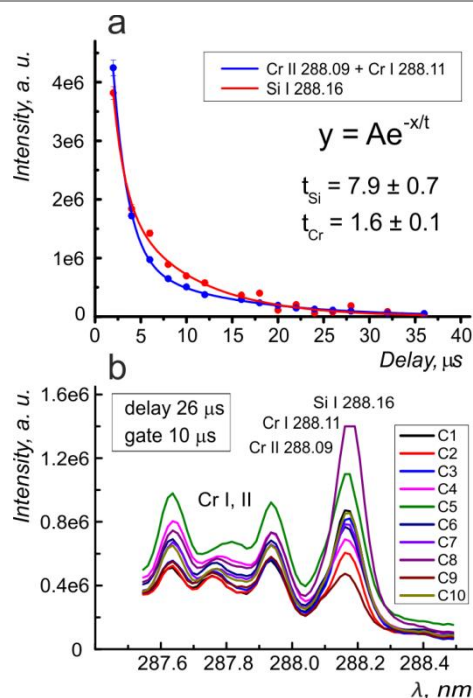


Figure 4. a) The dependencies of Si I line and sum of Cr II 288.09 and Cr I 288.11 lines on delay time. The parameters of exponential decay are given in a legend. b) Spectra of all samples in the range 287.5-288.5 nm.

Reducing the matrix effects with the use of an internal standard was impossible because there were no available individual lines of iron in this spectral window. We achieved the slight improvement of calibration by determining a baseline value as the value of the closest minimum in the blue region of the emission spectrum (see Table 2). The self-absorption was observed for the sample with the highest content of silicon (C8); therefore, we plotted a calibration curve without sample C8, and linearity was sufficiently better ( $R^2=0.88$ ). Since our attempts to improve the quality of univariate calibration with the use of Si I line at 288.16 nm did not lead to appropriate results, we considered the Si I line at 212.41 nm that had been previously used only as an internal standard in the LIBS quantification of phosphorus in ores<sup>22</sup> and carbon in coal.<sup>23</sup> There were no spectral interferences from iron and chromium. Although there was some overlapping with the wings of Ni I line at 212.14 nm, two individual peaks can be easily distinguished (see Figure 1,b). This led to sufficient high linearity of the calibration curve for the determination of silicon in high-alloy steels (see Figure 5,a). We used some individual lines of iron available in this spectral range as the internal standard, but this did not improve the calibration curve (see Table 2). Similar to Si I line at 288.16 nm some improvement in calibration was achieved with the exclusion of the C8 sample and setting a baseline level (Figure 6). Thus, to construct conventional calibration for silicon determining in high-alloyed

steels the use of Si I line at 212.41 nm provided the best result since it less affected by spectral interferences (see Figure 1,b). We chose the spectral range of 399-413 nm for the determination of manganese and chromium, where there are a number of their well-resolved lines as it was explicitly shown after modeling spectra within the range.<sup>24</sup> We examined Mn I 404.13 nm, Cr I 401.248 nm and Cr I 403.91 nm as analytical lines, and the resonance lines of manganese were not considered to avoid self-absorption. There was an interval within this spectral range without emission lines, where the light intensity corresponded to continuous background of the laser plasma. We have tried to use this value to reduce pulse-to-pulse variations of the laser plasma, but no significant changes (or even a worsening) of the calibration curve were observed, the same result was received with the subtracting of the baseline intensity (see Table 2). Since the normalization by the background radiation worsened calibration, we did not use it further. Here and after, the baseline corrected signals were used for internal standardization. The use of iron line Fe I 411.85 nm as an internal standard allowed the correction of matrix effects and the improvement of the calibration curve, so in the case of the coordinates normalized intensity to the ratio of manganese and iron contents the square of the linear correlation coefficient was 0.996 (see Figure 5,d). Similarly to manganese determination (with the use of cleaned signal, baseline correction and normalization to the internal standard) calibration curves were plotted for selected analytical lines of chromium (see Table 2). The best calibration was provided for the chromium line Cr I 403.91 nm normalized by Fe I 411.85 nm (see Figure 5,b).

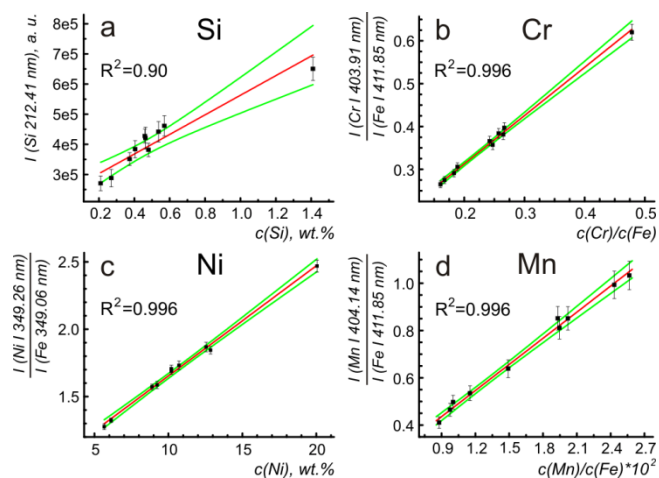


Figure 5. The best univariate calibration curves obtained for: a) Si, b) Cr, c) Ni, and d) Mn.

In the case of Ni determination, there are a lot of strong overlapped lines of Ni I and Ni II in the spectral range 210-220 nm. Only three nickel lines, which can be considered as isolated lines, e.g. Ni I 212.14 nm, Ni II 216.91 nm, and Ni II 217.51 nm, were examined to build univariate calibration curves. The prediction capabilities of several techniques, which were used for calculation of the analytical signal, are compared in Table

2. Cleaned intensities at each line provided better prediction than the intensities normalized by several reference iron lines ( $R^2 \sim 0.8-0.9$  vs  $0.4-0.8$ ). Since the quality of the calibration curve for Ni determination was not sufficient for analytical measurements, we examined the range of 345-365 nm, containing several isolated lines of Ni. For univariate

calibration we used Ni I 349.26 nm, 350.08 nm, 359.77 nm as analytical lines, and the Fe I 349.06 nm as an internal standard. These analytical lines provided good linearity of calibration curve after normalization by internal standard. The best calibration curve for Ni is shown in **Figure 5,c** ( $R^2=0.996$ ).

Table 2. The results for univariate calibration with the use of different normalization techniques.

Analytical signal	$R^2$	Analytical signal	$R^2$
Si		Ni	
Si I 212.41 nm (cleaned)	0.90	Ni I 212.14 nm – baseline	0.78
Si I 212.41 nm - baseline	0.92	Ni I 212.14 nm / Fe I 211.31 nm	0.44
Si I 212.41 nm / Fe I 211.31 nm	0.57	Ni I 212.14 nm / Fe I 213.97 nm	0.65
Si I 212.41 nm / Fe I 213.97 nm	0.65	Ni II 216.91 nm – baseline	0.87
Si I 212.41 nm / Fe I 217.26 nm	0.77	Ni II 217.51 nm (cleaned)	0.79
Si I 288.16 nm (cleaned)	0.86	Ni II 217.51 nm / Fe I 213.97 nm	0.76
Si I 288.16 nm - baseline	0.90	Ni I 349.26 nm (cleaned) & – baseline	0.82
Si 212.41 (cleaned) without C8	0.94	Ni I 350.08 nm (cleaned) & – baseline	0.91
Si 212.41 -baseline without C8	0.93	Ni I 359.77 nm (cleaned)	0.86
Si I 288.16 nm (cleaned) without C8	0.79	Ni I 359.77 nm – baseline	0.92
Si I 288.16 nm - baseline without C8	0.88	Ni I 349.26 nm / Fe I 349.06 nm	0.996
Cr		Ni I 350.08 nm / Fe I 349.06 nm	0.994
Cr I 401.248 nm - baseline	0.968	Ni I 359.77 nm / Fe I 349.06 nm	0.996
Cr I 401.248 nm / Fe I 401.453 nm	0.994	Ni I 349.26 nm / Fe I 349.06 nm vs. $c(\text{Ni}) / c(\text{Fe})$	0.96
Cr I 401.248 nm / Fe I 411.85 nm	0.966	Ni I 350.08 nm / Fe I 349.06 nm vs. $c(\text{Ni}) / c(\text{Fe})$	0.95
Cr I 401.248 nm / Fe I 401.453 nm vs. $c(\text{Cr}) / c(\text{Fe})$	0.986	Ni I 359.77 nm / Fe I 349.06 nm vs. $c(\text{Ni}) / c(\text{Fe})$	0.94
Cr I 401.248 nm / Fe I 411.85 nm vs. $c(\text{Cr}) / c(\text{Fe})$	0.993	Mn	
Cr I 403.91 nm - baseline	0.970	Mn I 404.13 nm (cleaned)	0.985
Cr I 403.91 nm / Fe I 411.85 nm	0.968	Mn I 404.13 nm (cleaned) / background	0.958
Cr I 403.91 nm / Fe I 401.453 nm	0.975	Mn I 404.13 nm / Fe I 411.85 nm	0.959
Cr I 403.91 nm / Fe I 411.85 nm vs. $c(\text{Cr}) / c(\text{Fe})$	0.996	Mn I 404.13 nm / Fe I 411.85 nm vs. $c(\text{Mn})/c(\text{Fe})$	0.996
Cr I 403.91 nm / Fe I 401.453 nm vs. $c(\text{Cr}) / c(\text{Fe})$	0.995	Mn I 404.13 nm – baseline	0.991

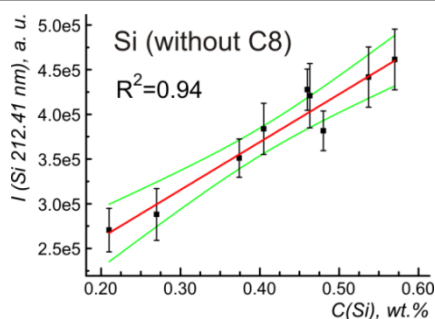


Figure 6. The improvement of univariate calibration curve for Si determination if sample C8 was dropped from a set of samples.

### Multivariate calibration

We applied PCR algorithm to construct a multivariate model for prediction of Ni, Si, Cr and Mn concentration. The main idea of the approach is a special decomposition of the matrix of signals  $X$ :

$$X = TL^t,$$

where  $T$  is a matrix of scores and  $L$  is a matrix of loadings. The detailed description of the procedure may be found elsewhere.<sup>25</sup> The narrow spectral windows containing the analytical lines of analytes were cut from the whole spectral range in order to obtain  $X$  matrices. The main parameter of the model is the

number of principal components (PC's, i.e. the number of significant column vectors in matrix  $T$ ). It is necessary to determine the number of PC's in order to avoid underfitting, which can lead to incorrect results of quantitative analysis. Leave-One-Out (LOO) cross-validation<sup>26</sup> procedure was used for estimation of robustness of constructed models. We slightly modified the ordinary minimizing Root-Mean-Square Error of Cross-Validation ( $RMSECV$ ) and replaced it with the relative  $RMSECV$  according to the expression:

$$RMSECV, \% = \frac{1}{n} \sum_{i=1}^n \frac{c_i - \bar{c}_i}{\bar{c}_i}^2,$$

where  $c_i$  and  $\bar{c}_i$  were the predicted concentration of component in the  $i$ -th sample and nominal ones, respectively, and  $n$  was the total number of samples under procedure LOO cross-validation. Two approaches to the determination of the optimal number of PC's were performed. In the first case, we took the number of PC's corresponding to the minimum of  $RMSECV, \%$  parameter as an optimum. Second approach was used to reduce the number of PC's in order to avoid an overfitting of the model. We applied  $F$ -criterion described in the paper<sup>26</sup> to a set of the samples involved in cross-validation procedure. A simple metrics based on prediction error sum of squares ( $PRESS$ ) representing a sum of squares  $\sum_{i=1}^n c_i - \bar{c}_i^2$  was used. The optimal number of PC's ( $h$ ) can be found from the metrics:

$$PRESS(h) \leq PRESS(h^*) < F_{m, m, 1-\alpha},$$

where  $h^*$  was the number of PC's corresponding to a minimum of the  $PRESS$ , and  $F_{m, m, 1-\alpha}$  was the coefficient of Snedecor's distribution with  $m=n-1$  degrees of freedom and probability  $1-\alpha$ . While the condition was true,  $h$  ( $h < h^*$ ) was reduced. We used  $\alpha=0.25$  in accordance with the recommendation of Haaland and Thomas<sup>26</sup> to avoid underfitting. It meant that the parameters  $PRESS(h)$  and  $PRESS(h^*)$  were differed with the probability  $(1-2\alpha) \times 100\% = 50\%$ . The results of our calculation are given in **Table 3**.

To improve the robustness of constructed models, we investigated the changes of the  $RMSECV, \%$  vs number of PC's besides searching for the minimum of relative  $RMSECV$  and the use of  $F$ -criterion. The prediction capabilities of the constructed models were differed strongly between two training sets of samples with and without sample C8. **Figure 7** illustrates both cases of Si prediction. For the complete set, the smooth trend of  $RMSECV, \%$  (**Figure 7,a**) cannot be obtained in the range of 212 nm, and unexpected minimum at 2 PC's is observed for the range of 288 nm. Thus, we supposed that models were unstable. The self-absorption of Si I lines (212.41 nm and 288.16 nm) for the sample C8 with the highest content of Si seemed to be a reasonable explanation of such observation. Therefore, we excluded the sample C8 from the procedure of LOO cross-validation. The smooth trend of the  $RMSECV, \%$  was obtained in the range of 212 nm (**Figure 7,b**). In the range of 288 nm the unexpected minimum at 2 PC's was remained.

Since there were several strong resonance lines of Si I in the range of 220 nm, this range was examined as a separate model. The results for Si prediction without sample C8 in the range of 220 nm (**Table 3**) were worsened significantly ( $R^2$  decreased from 0.88 to 0.55). Therefore, such model cannot be considered as a stable model too. Perhaps, the instability might be caused by two reasons: (i) the overlapping of many lines of Si with the lines of Ni and Fe, and (ii) relatively small signal of Si in comparison with other signals. Therefore, the most stable and best model for Si prediction was one constructed in the range of 212 nm with excluding the sample C8. **Figure 7,b** demonstrates the selection of the optimal number of PC's according to  $F$ -criterion. Minimum of  $RMSECV, \%$  in the right picture corresponds to 7 PC's, but the application of  $F$ -criterion resulted in that 4 PC's were enough. It means that the number of PC's can be reduced from 7 to 4 without essential worsening of prediction accuracy for both spectral ranges (288 nm and 212 nm).

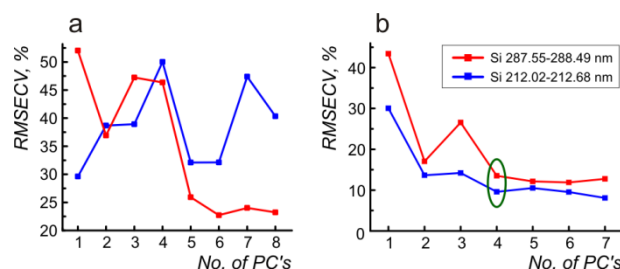


Figure 7. The evolution of  $RMSECV, \%$  for prediction of Si for all samples represents unstable models (a). The case of stable models without sample C8 is shown on the right (b).

It should be noted that the exclusion of sample C8 given slightly better results of the prediction of the Cr concentration in the range of 288 nm (see **Table 3**), but the models for Cr were also stable with sample C8. As opposite to Cr and Si cases, the prediction of Ni content for both spectral ranges was significantly worsened for sets without sample C8. However, exclusion of the sample C8 decreased twice the number of PC's. In **Figure 8**, the evolution of  $RMSECV, \%$  for Ni in the

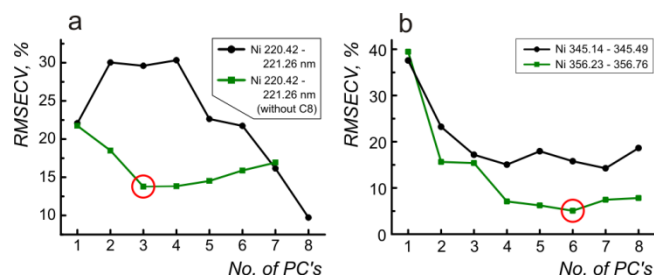


Figure 8. Selection of the stable model for prediction of Ni concentration and the optimal number of PC's for Ni: a) the range 220 nm b) the range 345 and 356 nm

range of 220 nm illustrates that the model without sample C8 was stable. The best model for Ni prediction with 6 PC's both  $F$  criterion restriction and without it was obtained in the range 356.23-356.76 nm (**Figure 8,b**), which included several unresolved lines (Fe I 356.54 nm, Ni I 356.64 nm and a number

of Cr I lines). But the model for Cr was unstable in this range for any number of PC's. This fact may be explained by overlapping of Cr I lines with different transition probabilities and excitation conditions which violated the additivity of

signals. We obtained a stable model with 4 PC's for Mn prediction either with F-criterion or without it (see **Figure 9**).

Table 3. The results of PCR prediction capabilities for Ni, Si, Cr and Mn concentrations.

Set of the samples	Spectral range, nm	No. of variables <sup>1</sup>	F-criterion	No. of PC's	RMSECV	RMSECV, %	R <sup>2</sup>	
<b>Ni</b>								
C1 – C10	212.02 – 212.68	43	no	6	1.4	14	0.88	
			yes	5	1.6	16	0.83	
	220.42 – 221.26	55	no	8	0.9	10	0.96	
			yes	8	0.9	10	0.96	
C1 – C7, C9, C10	212.02 – 212.68	43	no	5	1.8	17	0.82	
			yes	4	2.7	39	0.56	
	220.42 – 221.26	55	no	3	1.5	14	0.90	
			yes	3	1.5	14	0.90	
	C1 – C10	345.14 – 345.49	25	no	7	1.3	14	0.81
				yes	3	1.5	17	0.85
356.23 – 356.76		37	no	6	0.7	5	0.98	
			yes	6	0.7	5	0.98	
<b>Si</b>								
C1 – C10	212.02 – 212.68	43	no	1	0.3	30	0.33	
			yes	3	0.2	39	0.68	
	220.42 – 221.26	55	no	7	0.13	18	0.88	
			yes	7	0.13	18	0.88	
287.55 – 288.49	64	no	6	0.2	23	0.73		
		yes	5	0.2	26	0.60		
C1 – C7, C9, C10	212.02 – 212.68	43	no	7	0.04	8	0.90	
			yes	4	0.04	10	0.86	
	220.42 – 221.26	55	no	7	0.07	23	0.55	
			yes	1	0.10	34	0.23	
	287.55 – 288.49	64	no	6	0.04	12	0.87	
			yes	4	0.05	14	0.84	
<b>Cr</b>								
C1 – C10	287.55 – 288.49	64	no	8	0.6	3.4	0.975	
			yes	5	0.6	4.0	0.971	
	402.80 – 404.25	104	no	4	0.8	4.3	0.957	
			yes	4	0.8	4.3	0.957	
C1 – C7, C9, C10	287.55 – 288.49	64	no	7	0.5	3.1	0.987	
			yes	4	0.6	4.0	0.978	
C1 – C10	345.14 – 345.49	25	no	7	1.9	12	0.73	
			yes	5	2.0	14	0.72	
<b>Mn</b>								
C1 – C10	402.80 – 404.25	104	no	4	0.04	2.8	0.991	
			yes	4	0.04	2.8	0.991	

<sup>1</sup> the number of variables is the number of pixels in the wavelength region

The best results for the prediction of the elements are presented in **Figure 9**. To plot these figures, we choose the most stable model for each element, and the number of PC's corresponded to optimal ones with the use of the *F*-criterion. Procedures for

Mn and Cr determination provide reliable prediction accuracy and can be recommended as the analytical techniques for determination of these elements in high-alloyed steel. Perhaps, looking for an appropriate spectral range for Ni determination

can improve the prediction accuracy. We can recommend the range of 212 nm for silicon prediction, however, the additional optimization of experimental condition is needed to avoid the self-absorption of Si I line.

Lomonosov Moscow State University, Department of Chemistry, Leninskie Gory 1-3, Moscow, 119991, Russia, phone +7 495 939 36 35, e-mail timurla@laser.chem.msu.ru.

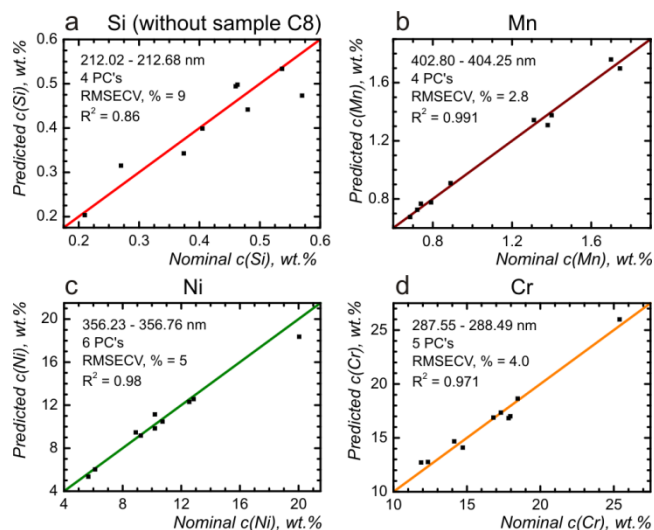


Figure 9. The best multivariate prediction plots obtained for Si, Mn, Ni, and Cr.

## Conclusions

We compared two calibration strategies (univariate and multivariate) for determination of Ni, Cr, Mn and Si in high-alloyed stainless steels. The different types of peak signal (cleaned, baseline corrected, corrected to internal standard) were used for plotting common univariate calibration curves. PCR was implemented for multivariate calibration. The use of line 212.41 nm for Si determination was better because self-absorption and spectral interferences were less than for the line at 288.16 nm. The best results for Cr, Ni and Mn ( $R^2=0.996$ ) were obtained with the use of common calibration with appropriate internal standard lines of iron. We can conclude that if the analyte signal is isolated in a varying degree by temporal separation of emission lines in LIBS spectrum, the univariate calibration with the using of appropriate internal standard is preferable because it gives better results. Multivariate calibration seems to be preferable with respect to the better prediction in the case of impossibility to separate signals anyway.

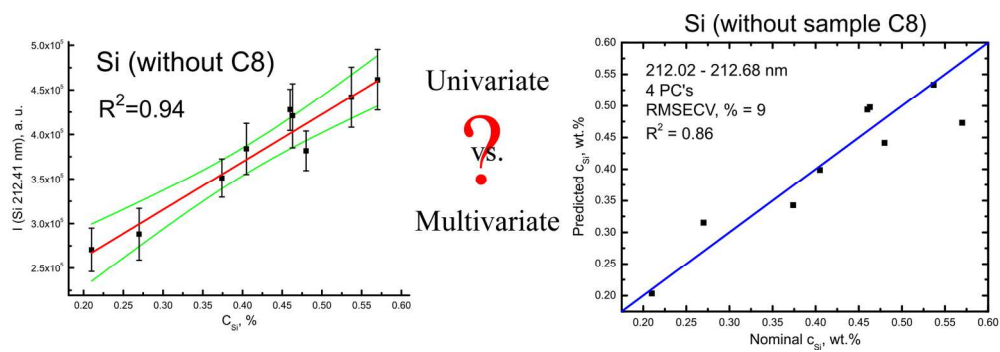
## Acknowledgements

We thank Dr. Andrey V. Garmash for the software for PCR analysis of experimental data. The work was financially supported by Russian Foundation for Basic Research (grants No. 14-03-31227-mol\_a, 13-03-13104-ofi\_m\_RzhD).

## Notes and references

- 1 D.W. Hahn and N. Omenetto, *Appl. Spectrosc.*, 2012, **66**, 347.
- 2 I. Gaona, J. Moros and J.J. Laserna, *J. Anal. At. Spectrom.*, 2013, **28**, 1750.
- 3 R. Noll, I. Mönch, O. Klein and A. Lamott, *Spectrochim. Acta Part B*, 2005, **60**, 1070.
- 4 S. Carter, A.S. Fisher, M.W. Hinds, S. Lancaster and J. Marshall, *J. Anal. At. Spectrom.*, 2013, **28**, 1814.
- 5 B. Zhang, L.X. Sun, H.B. Yu, Y. Xin and Z.B. Cong, *J. Anal. At. Spectrom.*, 2013, **28**, 1884.
- 6 B. Zhang, H.B. Yu, L.X. Sun, Y. Xin and Z.B. Cong, *Appl. Spectrosc.*, 2013, **67**, 1087.
- 7 N.B. Zorov, A.A. Gorbatenko, T.A. Labutin and A.M. Popov, *Spectrochim. Acta Part B*, 2010, **65**, 642.
- 8 J. Westberg, J.Y. Wang and O. Axner, *J. Quant. Spectrosc. Radiat. Transfer.*, 2012, **113**, 2049.
- 9 J. Vrenegor, R. Noll and V. Sturm, *Spectrochim. Acta Part B*, 2005, **60**, 1083.
- 10 T. Yuana, Z. Wang, Z. Lia, W. Nia and J. Liu, *Anal. Chim. Acta.*, 2014, DOI: 10.1016/j.aca.2013.11.027.
- 11 P.M. Mukhono, K.H. Angeyo, A. Dehayem-Kamadjeu and K.A. Kaduki, *Spectrochim. Acta Part B*, 2013, **87**, 81.
- 12 F.C. De Lucia and J.L. Gottfried, *Appl. Optics*, 2012, **51**, B83.
- 13 J. Moros, J. Serrano, C. Sanchez, J. Macias and J.J. Laserna, *J. Anal. At. Spectrom.*, 2012, **27**, 2111.
- 14 M. Hoehse, A. Paul, I. Gornushkin and U. Panne, *Anal. Bioanal. Chem.*, 2012, **402**, 1443.
- 15 Q. Godoi, F.O. Leme, L.C. Trevizan, E.R. Pereira, I.A. Rufini, D. Santos and F.J. Krug, *Spectrochim. Acta Part B*, 2011, **66**, 138.
- 16 C.B. Stipe, B.D. Hensley, J.L. Boersema and S.G. Buckley, *Appl. Spectrosc.*, 2010, **64**, 154.
- 17 F. Sorrentino, G. Carelli, F. Francesconi, M. Francesconi, P. Marsili, G. Cristoforetti, S. Legnaioli, V. Palleschi and E. Tognoni, *Spectrochim. Acta Part B*, 2009, **64**, 1068.
- 18 E.V. Thomas and D.M. Haaland, *Anal. Chem.*, 1990, **62**, 1091.
- 19 P. Yaroshchuk, D.L. Death and S.J. Spencer, *J. Anal. At. Spectrom.*, 2012, **27**, 92.
- 20 J. Engel, J. Gerretzen, E. Szymańska, J.J. Jansen, G. Downey, L. Blanchet and L.M.C. Buydens, *Trends Anal. Chem.*, 2013, **50**, 96.
- 21 E. Tognoni, V. Palleschi, M. Corsi and G. Cristoforetti, *Spectrochim. Acta Part B*, 2002, **57**, 1125.
- 22 G. Asimellis, A. Giannoudakos and M. Kompitsas, *Spectrochim. Acta Part B*, 2006, **61**, 1253.

- 1  
2  
3  
4  
5  
6  
7  
8  
9  
10  
11  
12  
13  
14 23 S. Yao, J. Lu, J. Zheng and M. Dong, *J. Anal. At. Spectrom.*, 2012,  
15 27, 473.  
16 24 T.A. Labutin, S.M. Zaytsev and A.M. Popov, *Anal. Chem.*, 2013, **85**,  
17 1985.  
18 25 M. Otto, *Chemometrics. Statistics and Computer Application in*  
19 *Analytical Chemistry*, Wiley, Weinheim, 2007.  
20 26 D. Haaland and E. Thomas, *Anal. Chem.*, 1988, **60**, 1193.  
21  
22  
23  
24  
25  
26  
27  
28  
29  
30  
31  
32  
33  
34  
35  
36  
37  
38  
39  
40  
41  
42  
43  
44  
45  
46  
47  
48  
49  
50  
51  
52  
53  
54  
55  
56  
57  
58  
59  
60



168x56mm (299 x 299 DPI)

1  
2  
3  
4  
5  
6  
7  
8  
9  
10  
11  
12  
13  
14  
15  
16  
17  
18  
19  
20  
21  
22  
23  
24  
25  
26  
27  
28  
29  
30  
31  
32  
33  
34  
35  
36  
37  
38  
39  
40  
41  
42  
43  
44  
45  
46  
47  
48  
49  
50  
51  
52  
53  
54  
55  
56  
57  
58  
59  
60

Overcoming matrix effect on LIBS analysis of high-alloyed stainless steel by specifying the temporal parameters of signal registration and multivariate calibration based on principal component regression (PCR) have been evaluated.